Available online at www.sciencedirect.com
SCIENCE DIRECT
Catalysis Today 114 (2006) 217–225
CATALYSIS TODAY
www.elsevier.com/locate/cattod

# Steam and acid dealumination of mordenite Characterization and influence on the catalytic performance in linear alkylbenzene synthesis

Marcelo Boveri [a], Carlos Márquez-Álvarez [a], Miguel Ángel Laborde [b], Enrique Sastre [a,*]

[a] *Instituto de Catálisis y Petroleoquímica, C.S.I.C., c/Marie Curie 2, Cantoblanco, 28049 Madrid, Spain*
[b] *Departamento de Ingeniería Química (FI), Universidad de Buenos Aires, Pabellón de Industrias, Ciudad Universitaria, 1428 Buenos Aires, Argentina*

Available online 14 February 2006

**Abstract**

A systematic study of both acid and steam dealumination of mordenite has been carried out aiming to obtain a mordenite featuring high acid strength active sites along with a secondary mesoporous system, in order to maximize both catalytic performance and time-on-stream stability of the material in solid-acid catalyzed alkylation of benzene with 1-dodecene. Detailed assessment of the textural (XRD, $N_2$ adsorption–desorption) and acid (FTIR of pyridine adsorption) properties of the obtained materials was performed.

It has been found that catalysts obtained by combined steam dealumination and acid washing show a dramatic increase in the intrinsic activity and a significantly lower tendency to suffer deactivation when compared to the parent zeolite and samples obtained by acid treatments. This improved behaviour of the steam-treated sample is attributed to its increased mesoporous surface area, lower acid sites concentration and less hydrophilic surface.


*Keywords:* Mordenite; Acid dealumination; Steam dealumination; Linear alkylbenzene

## 1. Introduction

Mordenite is a silica-rich, large pore zeolite, which features a series of parallel 12-MR elliptical channels with dimensions of ca. 0.67 × 0.70 nm parallel to the *c* axis, as well as smaller 8-membered *side pockets* with dimensions of ca. 0.29 × 0.57 nm. Being the latter channels too small to allow molecules to diffuse through them from one main channel to another, the resulting structure is considered de facto unidirectional.

Mordenite differs from other zeolites in that a large amount of aluminium can be readily removed without substantial loss in crystallinity [1]. Mild acid dealumination of H-MOR was reported to result in a more active catalyst [2–4] due to the removal of amorphous material from the structure channels, as well as the generation of stronger acid sites during the dealumination process. Under specific dealumination conditions, this leads to both activity and selectivity improvements for particular reactions. Such effect was ascribed to the presence of fewer and stronger Brønsted acid sites. After steaming, however, mordenite samples were reported to show less activity, this being ascribed to the elimination of acid sites and increased diffusional resistance caused by the deposition of extraneous material within the pores [4].

Linear alkylbenzenes were introduced in the mid-1960s as raw material for synthetic detergents, replacing the former, environment-unfriendly, branched alkylbenzenes. It became soon clear that the liquid acid, state-of-the-art manufacturing technology brought about serious safety and environment concerns. The strong acidity shown by zeolites made them potentially appealing materials in terms of activity and selectivity to the desired monoalkylbenzenes in order to replace the Friedel–Crafts catalysts by solid acids. In an early work in 1966, Venuto et al. studied rare earth-exchanged X and Y zeolites as catalysts for the alkylation of benzene with

* Corresponding author. Fax: +34 91 585 4760.
*E-mail address:* esastre@icp.csic.es (E. Sastre).

0920-5861/$ – see front matter © 2006 Elsevier B.V. All rights reserved.
doi:10.1016/j.cattod.2006.01.012

1-decene [5]. From that time, abundant studies were carried out employing diverse structures, namely FAU [2,5–12,15,17], MFI [2,7,17], BEA [6,10,11,13,14], MOR [2,10,11,14,16–19] and EMT [6,11]. The diversity of regular confined space systems yielded by the different available zeolite frameworks offered the possibility to achieve shape-selectivity effects in order to shift the isomer distribution of the reaction products to the readily biodegradable and more soluble 2- and 3-phenylalkanes. Amongst the many zeolite structures tested, MOR has shown a good activity along with an outstanding selectivity to the desired phenylalkanes.

The aim of the present work is to perform a systematic investigation on the effect that acid and steam dealumination treatments of mordenites have on their structure, acidic properties and catalytic behaviour in linear alkylbenzenes synthesis.

## 2. Experimental

Parent material was an $NH_4$-MOR from Zeolyst International (CBV 21A), with a Si/Al ratio = 10. The acidic form of the parent zeolite, labeled M0, was obtained by calcination of CBV 21A in the conditions described below.

Acid treatment of the zeolites was carried out by stirring a suspension of the solid plus 20 ml of HCl solution of a given concentration per gram of solid within a reflux-attached round bottom flask at 363 K for 16 h. After that, solid was filtered and washed with distilled water repeatedly until total chloride removal. In order to carry out the acid-borne dealumination of the materials, successive treatments were performed up to three times with 6 M HCl, followed by a final treatment with 8 M HCl. Samples were labeled MH*x*, with *x* being 1, 2, 3 after the number of 6 M HCl treatments, or '*F*' after the 8 M HCl treatment. Samples were calcined after their last acid treatment.

Calcination of the materials was performed in air under a 3 K $min^{-1}$ temperature program with isothermal stages at 413 K (2 h), 573 K (2 h) and at 813 K (4 h).

Steaming of the parent zeolite was carried out at 873 K for 6 h in air under a 10 ml $min^{-1}$ steam flow. During the steam treatment, aluminum hydrolyzes and migrates to cationic positions, neutralizing framework acid sites, so steamed material aliquots were treated with 3 and 6 M HCl solutions for 4 h using the aforementioned procedure. Samples were labeled MS, MS3 and MS6, respectively.

XRD powder diffraction patterns of the samples containing 7–10 wt.% water were recorded on a Seifert XRD 3000, using Cu Kα radiation and operating within the $4^\circ < 2\theta < 40^\circ$ range. Crystallinity of the samples was assessed as the sum of the areas of the [1 5 0], [2 0 2] and [3 5 0] reflections, relative to the parent zeolite.

Chemical Al and Si analyses of the materials were obtained by inductively coupled plasma atomic emission spectroscopy (ICP-AES) using a Winlab Optima 3300 DV ICP spectrometer from Perkin-Elmer. Samples were previously dried at 383 K. Disgregation of the sample was obtained by alkaline fusion in an automatic fusion device Fluxy-30 from Claisse using a 50/50 wt.% fusion mixture of $Li_2B_4O_7$ and $LiBO_2$. Fused mixtures were demolded using KI and collected in a 10 wt.% $HNO_3$ solution.

Nitrogen adsorption–desorption isotherms were obtained using a Micromeritics ASAP 2000 device. Specific surface area and micropore volume were calculated by the $\alpha_S$-plot method.

For infrared measurements, the sample was pressed into thin self-supporting wafer (thickness, ca. 8 mg $cm^{-2}$) and activated in vacuum ($10^{-3}$ Pa) at 623 K for 9 h in a glass IR cell with $CaF_2$ windows. Pyridine (analytical grade, Fluka) was dosed (8 Torr) at room temperature and successive evacuation treatments at 423, 523 and 623 K for 1 h under dynamic vacuum were performed. Infrared spectra were recorded after activation and after each evacuation treatment using a Nicolet 5ZDX FTIR spectrometer provided with an MCT detector. Spectra in the 4000–1000 $cm^{-1}$ range were acquired at 4 $cm^{-1}$ resolution by averaging 250 scans and using Happ–Genzel apodization.

Catalytic tests were carried out in a Parr 100 ml stirred batch reactor. Reagents mixture composition was benzene and 1-dodecene (10:1 molar ratio) plus 2.5 wt.% catalyst. Tetradecane was employed as an internal standard (10 wt.%). Reagents employed were 1-dodecene (Tech. grade) 96% from Alfa, benzene (dry) from Panreac and *n*-tetradecane 99% from Sigma, which were kept dry with 0.5 nm molecular sieve by Panreac.

The reactor was loaded with the total amounts of benzene, tetradecane and catalyst, the atmosphere was purged with dry nitrogen and the system was heated up to the desired reaction temperature. At that time, the olefin was pulse-injected into the system and the pressure was set to 0.5 MPa with nitrogen.

Aliquots of the reacting mixtures were periodically taken and analyzed by GC in a Fisons 8000 Series device, with a Tracer™ capillary column coated with Tracsil-TR-WAX, with 60 m × 0.25 mm × 0.25 μm dimensions, connected to a FID detector, with helium as carrier gas.

Phenyldodecane isomers were identified by GC–MS preliminary experiments. Calibrations were carried out with 1-phenyldodecane 97% from Avocado, assuming a constant mass-response of the FID signal for all phenyldodecane isomers.

## 3. Results and discussion

### 3.1. Characterization of treated materials

#### 3.1.1. Elemental analysis

Table 1 shows the effect of successive acid treatments of the parent mordenite. A massive Al leaching is observed after the first treatment, followed by a minor removal after the second one. Successive treatments with either 6 or 8 M acid solutions yield no important modifications in the Al content of the materials.

On the other hand, the steam-treated material MS shows a similar Al content to that of the parent material. Treatments with 3M (MS3) or 6M (MS6) acid solutions, yield substantially different Al contents, suggesting that Al segregated species formed during the steaming treatment are not readily removable.

Table 1
Aluminum content measurements for the samples at diverse treatment stages

| Sample | Si/Al[a] | Al[b] |
|---|---|---|
| M0 | 10 | 1.51 |
| MH1 | 55 | 0.30 |
| MH2 | 79 | 0.21 |
| MH3 | 87 | 0.19 |
| MHF | 92 | 0.18 |
| MS | 9.5 | 1.61 |
| MS3 | 18 | 0.89 |
| MS6 | 38 | 0.43 |

[a] Atomic ratio, by ICP-AES.
[b] mmol $g^{-1}$.

### 3.1.2. X-ray diffraction patterns

When crystallinity of the acid-treated samples is assessed, it can be seen that a loss occurs after the first acid treatment, with no further appreciable changes (Table 2). A very slight unit cell contraction, observed as a shrinkage of the *a* and *b* cell-parameters, also occurs during the first acid treatment, with no further contraction observed.

After the steam treatment, loss in crystallinity of similar magnitude to the one yielded by the first acid treatment is observed, while the resulting unit cell size lies in between those of the parent material and the acid-treated samples. Upon successive, high-concentration acid treatment of the steamed sample, crystallinity increase could be expected due to an intensive extra-lattice Al leaching. However, this is not the case, as samples MS and MS6 show similar crystallinity values (Table 2). Unit cell size remains unchanged through the post-steaming acid treatment.

### 3.1.3. Acidity of materials

The acid properties of mordenites were analyzed by FTIR spectroscopy. Infrared spectra of calcined samples activated in vacuum at 673 K are shown in Fig. 1, in the region of hydroxyl stretching. The spectrum of the parent zeolite M0 shows three bands. The medium intensity band at 3745 $cm^{-1}$ is characteristic of terminal silanol groups located at the external surface of the zeolite crystals, while the broad, strong bands at ca. 3656 and 3608 $cm^{-1}$ are attributed to Al-OH moieties in extraframework aluminium and to the acidic bridging hydroxyls,

Table 2
Evolution of crystallinity and unit cell size for treated materials

| Sample | Crystallinity (%) | Unit cell parameter[a] | | | Unit cell volume[b] |
|---|---|---|---|---|---|
| | | *a* | *b* | *c* | |
| M0 | 100 | 1.815 | 2.035 | 0.749 | 2.765 |
| MH1 | 87 | 1.810 | 2.022 | 0.747 | 2.733 |
| MH2 | 86 | – | – | – | – |
| MH3 | 89 | – | – | – | – |
| MHF | 92 | 1.809 | 2.021 | 0.747 | 2.730 |
| MS | 85 | 1.811 | 2.030 | 0.747 | 2.746 |
| MS6 | 83 | 1.811 | 2.031 | 0.747 | 2.747 |

[a] In nm.
[b] In $nm^3$.

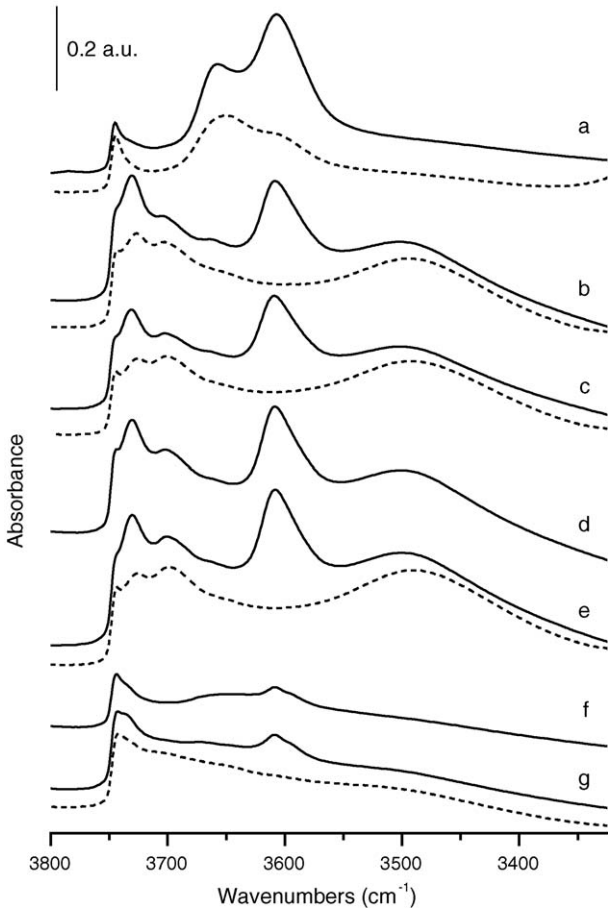


Fig. 1. Infrared spectra of samples M0 (a), MH1 (b), MH2 (c), MH3 (d), MHF (e), MS3 (f) and MS6 (g). Full lines correspond to spectra of activated samples and dotted lines to spectra recorded after pyridine adsorption followed by desorption at 423 K. The spectra have been normalized to a sample thickness of 7.5 mg $cm^{-2}$, corresponding to a wafer weight of 10 mg of sample on a dry basis.

respectively [20–23]. Acid leaching treatment of the zeolite produces the removal of extraframework aluminium, as indicated by the large decrease of intensity of the band at 3656 $cm^{-1}$ observed for MH samples, compared to the parent zeolite (Fig. 1). The acid leaching also produces a partial loss of intensity of the bridging hydroxyl band, and the developing of bands at ca. 3730, 3700 and 3500 $cm^{-1}$. Similar results have been previously reported for acid-leached H-mordenite [24]. The bands at 3730 and 3700 $cm^{-1}$ seem to be present as shoulders in the parent zeolite spectrum (careful inspection of the infrared spectra of mordenite samples reported in the literature reveals that both shoulders are common features in these spectra). Therefore, the acid treatment would enhance both bands. It is important to notice that the intensity of all the hydroxyl bands is very similar for all the MH samples, indicating that only small changes in the dealumination and hydroxylation degree occur as the number of acid leaching steps increases.

The band at 3700 $cm^{-1}$ has been assigned to silanol groups on defect sites, while the very broad band at 3500 $cm^{-1}$ would correspond to strongly interacting silanol groups [24]. The developing of both bands, as well as the partial loss of the

bridging hydroxyls band (3608 $cm^{-1}$) is consistent with the proposed mechanism of aluminium removal by the acid treatment [25]. The dealumination treatment produces the cleavage of Si–O–Al bonds, thus removing acidic hydroxyl groups and creating up to four internal, non-acidic silanol groups per each aluminium atom removed. However, partial condensation of these silanol groups has been shown to occur as the dealumination degree increases [26]. On the other hand, the acid treatment also gives rise to the growth of the band at 3730 $cm^{-1}$. This band can tentatively be assigned to hydroxyl groups on extraframework tetrahedral aluminium species, to which a $^{27}Al$ NMR peak at a chemical shift of ca. 100 ppm has been assigned [4] or, alternatively, to partial cleavage of the Si–O–Al bonds in $AlO_4$ tetrahedra. This assignment would be supported by the acidic behaviour exhibited by this hydroxyl group (vide infra).

The spectrum of sample MS6, prepared by steaming followed by acid washing with 6 M HCl solution, exhibits remarkable differences with respect to those of the acid-leached samples (Fig. 1). The steaming of the parent zeolite largely decreases the number of bridging hydroxyls and, therefore, the number of acid sites. The band at 3608 $cm^{-1}$ shows a very low intensity for the MS6 sample. Due to this low intensity, a second band can be identified as a shoulder at ca. 3595 $cm^{-1}$. The asymmetric band that is observed in the spectra of M0 and MH samples indicates the presence of two distinct bridging hydroxyls also in these samples, in agreement with earlier reports [26]. Compared to the acid-leached samples, the spectrum of the MS6 sample also shows a less intense 3730 $cm^{-1}$ band, while the bands at 3700 and 3500 $cm^{-1}$ are nearly absent. This result is in agreement with the proposed mechanism for steam dealumination [27], in which the silanol groups produced by the removal of aluminium condense to form Si–O–Si bonds. The difference in the dealumination mechanism therefore results in a much lower hydroxylation degree in the case of the steamed sample, compared to the acid-leached zeolites. Such a low hydroxylation degree is expected to result in a significant decrease of the hydrophilicity by the steaming treatment as compared to the acid leaching.

As in the case of the acid-leached samples, the band assigned to hydroxyl groups on extraframework aluminium (3656 $cm^{-1}$) is virtually absent after the steaming treatment followed by acid washing with 6 M HCl solution (Fig. 1). The spectrum of sample MS3 exhibits a broad band at ca. 3655 $cm^{-1}$, which reveals that extraframework aluminium species are not completely removed when the acid washing is carried out using a 3 M HCl solution. This result suggests that the aluminium cation aquocomplexes that are generated by steam dealumination might not be completely removed when using the less severe acid washing procedure. The lower intensity shown by the bridging hydroxyl bands in the spectrum of the MS3 sample compared to that of MS6 (Fig. 1) suggests that this is indeed the case. When a 3 M HCl solution is used, part of the aluminium cation aquocomplexes would remain in the sample as charge-compensating cations, and therefore decrease the number of Brønsted acid sites generated during the calcination.

In order to evaluate the concentration of acid sites, pyridine adsorption analysis by FTIR was performed. The total number of acid sites was determined by pyridine adsorption and subsequent degassing at 423 K.

The spectra recorded after this adsorption treatment have been plotted in Fig. 1. It can be observed that due to pyridine protonation by the Brønsted sites, the bands assigned to bridging hydroxyls are removed. Only for the parent M0 sample a band at 3608 $cm^{-1}$ is observed after pyridine adsorption, thus indicating that part of the Brønsted acid sites are not accessible to pyridine in this zeolite. For all the samples, pyridine adsorption also produces a decrease in the intensity of the bands at 3730 and 3656 $cm^{-1}$ (attributed to non-bridging Al-OH groups). This result evidences that these centres also contribute to the overall acidity of the samples, in agreement with sorption studies by Karge and Dondur [28], that revealed the presence of two Brønsted-type sites in dealuminated mordenites. In contrast, the silanol bands at 3745, 3700 and 3500 $cm^{-1}$ are not apparently affected by pyridine adsorption.

The concentration of Brønsted, as well as Lewis acid sites, and the distribution of acid sites strength have been evaluated by determining the intensity of bands of adsorbed pyridine after subsequent evacuation treatments at 423, 523 and 623 K. Fig. 2 shows difference spectra of selected samples, recorded after pyridine adsorption and subsequent degassing, and Table 3 collects the integrated absorbances of the bands at 1546 and 1455 $cm^{-1}$, corresponding to pyridine adsorbed on Brønsted and Lewis sites, respectively.

As shown in Table 3, the concentration of Lewis sites remains nearly constant through the successive degassing treatments, while that of Brønsted sites decreases as the evacuation temperature increases. The results indicate that around 50% of the Brønsted acid sites are strong sites, able to retain pyridine after evacuation at 623 K. The acid leaching treatment decreases the amount of acid sites. Around half of the acid sites are lost when the parent M0 zeolite is treated once with the 6 M HCl solution (sample MH1). In agreement with

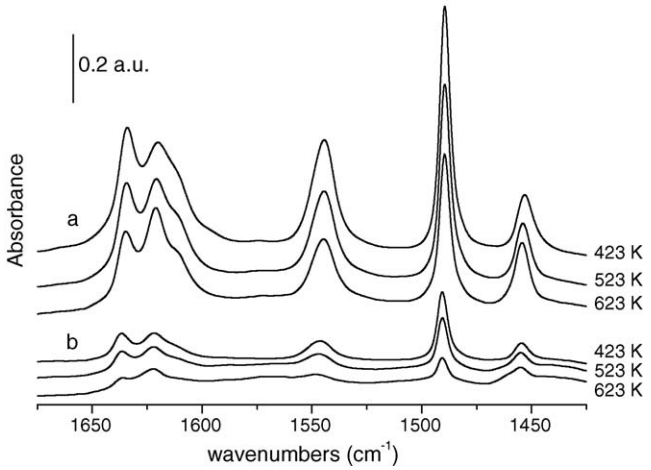


Fig. 2. Difference spectra of samples M0 (a) and MS6 (b) after pyridine adsorption followed by desorption at 423, 523 and 623 K in vacuum. The spectrum of the corresponding activated sample has been subtracted to every spectrum.

Table 3
Surface acidity determined by FTIR analysis of adsorbed pyridine

| Sample | Brønsted sites[a] (cm g$^{-1}$) | | | Lewis sites[a] (cm g$^{-1}$) | | | Total acidity[b] (mmol g$^{-1}$) |
|---|---|---|---|---|---|---|---|
| | 423 K | 523 K | 623 K | 423 K | 523 K | 623 K | |
| M0 | 620 | 491 | 354 | 217 | 203 | 231 | 0.47 |
| MH1 | 349 | 257 | 160 | 171 | 156 | 196 | 0.27 |
| MH2 | 304 | 255 | 143 | 133 | 127 | 158 | 0.23 |
| MHF | 358 | 276 | 165 | 112 | 117 | 143 | 0.27 |
| MS6 | 108 | 69 | 28 | 54 | 54 | 55 | 0.09 |

[a] Integrated absorbance normalized by the sample thickness of the IR bands of pyridine adsorbed on Brønsted (1546 cm$^{-1}$) and Lewis (1455 cm$^{-1}$) acid sites after degassing at various temperatures.
[b] Total amount of Brønsted and Lewis acid sites determined after vacuum treatment at 423 K, using the molar extinction coefficients reported in ref. [29].

results shown in Fig. 1 discussed above, the subsequent acid treatments only produce a small decrease in the acid sites concentration. On the other hand, a much more marked decrease of the concentration of acid sites is produced by the steaming treatment, as was already pointed out by comparing the intensities of the bridging hydroxyl bands. Aiming to estimate the total acidity of these mordenites (Table 3), we have calculated the concentration of Brønsted and Lewis sites by using the molar absorption coefficients reported in [29]. Even though the molar absorption coefficients for pyridine bound to Brønsted and Lewis sites reported in the literature differ significantly [30], we consider that the order of magnitude of the acidity values reported in Table 3 is correct.

### 3.1.4. Nitrogen isotherms

Nitrogen isotherms of all samples are characteristic of microporous materials which possess some mesoporosity. A H4 IUPAC-type hysteresis loop with a very steep step in the desorption branch occurring at $p_{rel} \approx 0.46$ appears for all the samples. Such step is related to the adsorbate surface tension at the analysis conditions, rather than to the textural properties of the adsorbent [31], thus interpretations in terms of mesopore distributions should take careful account of its nature in order not to be misleading. As an example, isotherms for the parent material and the steam-acid treated material MS6 both with steps at $p_{rel} = 0.46$ are shown in Fig. 3.

Also careful appreciations should be made about the evaluation and meaning of the BET surface area for microporous materials. The micropore filling mechanisms are clearly distinct from the multilayer proposed by the BET calculations, thus leading to materials with high *C*-values, for which the statistic monolayer capacity concept starts to suffer from increasing uncertainty. No valid linear ranges were found neither with the traditional equation nor with the variation developed by Keii and Tagaki [32] for materials with high *C*-values.

Relative isotherm plots have been proven to be useful tools in order to assess the textural properties of porous materials. Therefore, the $\alpha_S$-plots relative to a LiCrosspher-1000 silica standard published in the literature [33] have been obtained in order to measure the non-microporous surface area, i.e. the sum of mesoporous plus external surface areas. In Fig. 4, the $\alpha_S$-plot conversion of acid (A) and steam-acid (B) treated samples are

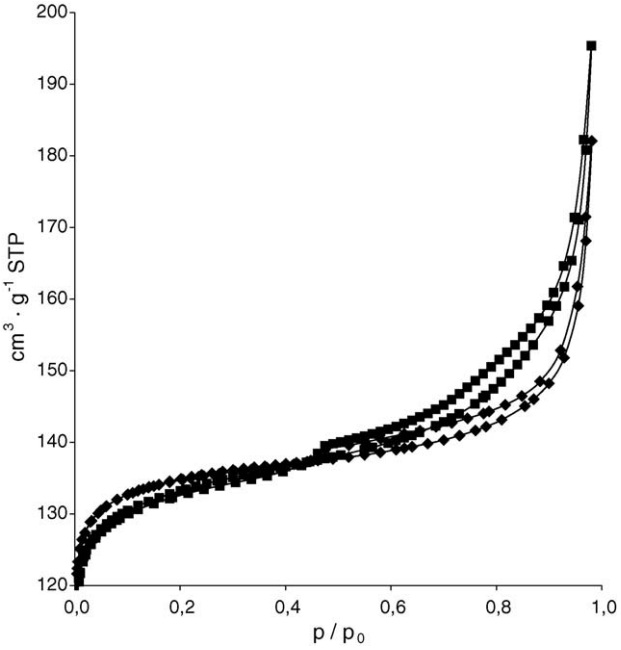


Fig. 3. Nitrogen adsorption-desorption isotherms of the parent material (M0, ◆) and a steam-acid treated sample (MS6, ■).

compared with that of the parent material. In all of them, it can be seen a first convex zone occurring at low $\alpha_S$ values, which corresponds to the micropore filling, followed by a linear zone at ca. $0.8 < \alpha_S < 1.3$, due to multilayer adsorption on the mesoporous and external area once the micropores are filled. Finally, a concave zone, attributed to a capillary condensation mechanism within a broad mesopore distribution occurs at $\alpha_S > 1.3$. In all cases, the linear zone can be expressed by the following equation: $V^{STP} = A_{rel} \times \alpha_S + V_\mu^{STP}$, where the slope corresponds to the ratio of the mesopore and external surface area of the sample to the surface area of the standard (the latter calculated by the BET procedure), and the intercept corresponds to the micropore volume in STP. Table 4 shows the so-calculated textural properties for the acid-treated samples, as well as the steam-acid treated materials together with the total pore volume as measured by the nitrogen uptake at $p_{rel} \approx 0.99$. It can be seen that acid treatment yields little changes in the textural properties of the materials. On the other hand, the steam treated sample experiences a noticeable micropore blockage and a small decrease of the non-microporous surface area. A 3 M HCl successive treatment retrieves both original parent material values, while the 6 M HCl treated material adds a noticeable higher non-microporous surface area. This fact can be seen in Fig. 4, as the increase in the slope of the linear zone of the MS6 $\alpha_S$-plot leads to a crossing with the parent material plot.

### 3.1.5. Catalytic activity

The effect of dealumination of mordenites on the alkylation of benzene with 1-dodecene, has been assessed at 373 K. In Fig. 5, the activity plots for the acid-dealuminated samples (A) and for the steam-acid treated materials (B) are shown, compared to the parent zeolite.

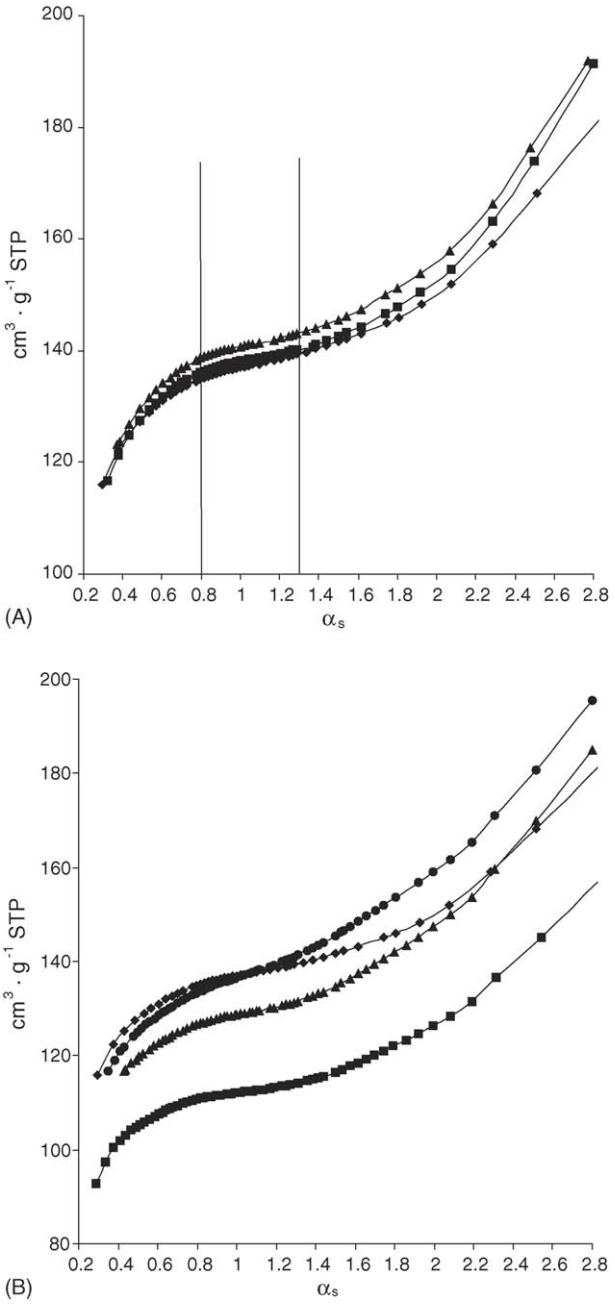


Fig. 4. $\alpha_S$-plots of chosen acid-treated (A) and steam-acid treated (B) samples, compared to the parent material: (A) M0, ◆; MH2, ■; MHF, ▲. (B) M0, ◆; MS, ■; MS3, ▲.; MS6, ●.

Table 4
Evolution of the microporous, mesoporous plus external and total pore volume and mesoporous plus external surface area of samples

| Sample | Pore volume [$cm^3\ g^{-1}$] | | | Surface area [$m^2\ g^{-1}$] |
|---|---|---|---|---|
| | Total | Microporous | Mesoporous + external | Mesoporous + external |
| M0 | 0.282 | 0.199 | 0.083 | 211 |
| MH2 | 0.296 | 0.203 | 0.093 | 177 |
| MHF | 0.297 | 0.205 | 0.092 | 201 |
| MS | 0.243 | 0.164 | 0.079 | 148 |
| MS3 | 0.286 | 0.186 | 0.100 | 208 |
| MS6 | 0.302 | 0.187 | 0.116 | 397 |

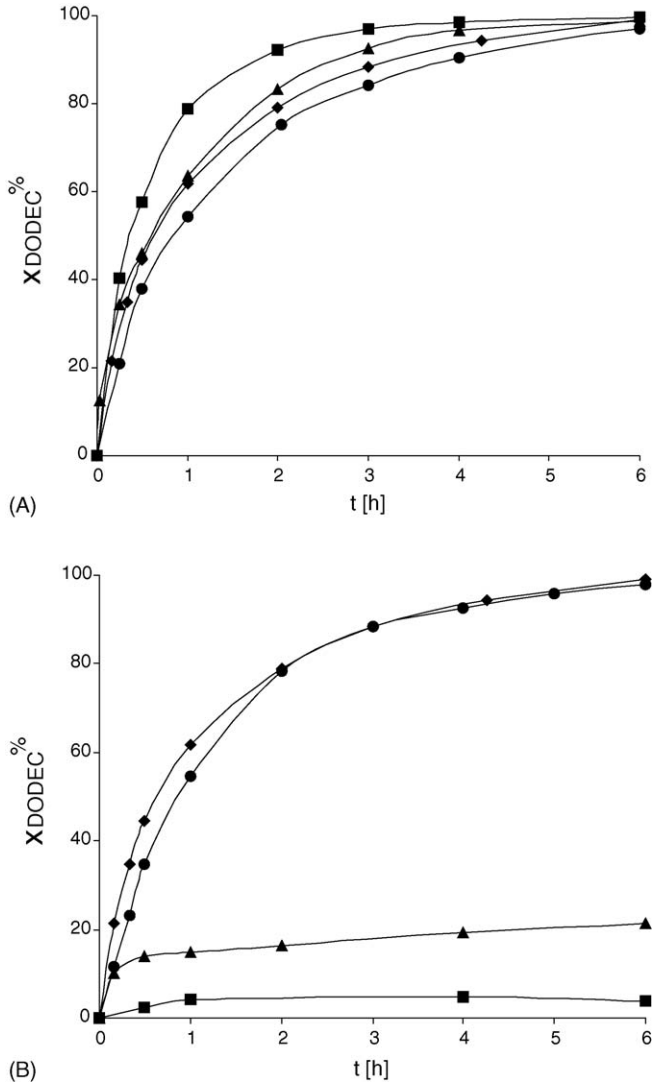


Fig. 5. Catalytic activity of acid-treated (A) and steam-acid treated (B) samples, compared to the parent material: (A) M0, ◆; MH1, ■; MH2, ▲; MHF, ●. (B) M0, ◆; MS, ■; MS3, ▲; MS6, ●.

It stands clear that acid treatment always yields active materials, whereas steam treatment yields an extremely low activity material, which only retrieves its activity after treatment with 6 M HCl solution.

Table 5 shows the results of the catalytic performance of these materials. No effect in neither yield to linear phenyldodecanes ($\eta_{LAB}$) nor selectivity to 2-phenyldodecane ($\sigma_{2\phi}$), expressed as the mass ratio of 2-phenyldodecane to the sum of all five phenyldodecane isomers, is achieved by the acid treatment. An improvement in the intrinsic activity per acid site (TOF), as measured by pyridine adsorption (Table 5) after the first acid treatment is also qualitatively seen in the time-conversion plot (Fig. 5A), as the MH1 sample shows a noticeable improvement in terms of dodecene conversion ($x_{DODEC}$) rate when compared to the parent material even

Table 5
Catalytic performance of the samples at 373 K, expressed as dodecene conversion ($x_{DODEC}$), yield to linear phenyldodecanes ($\eta_{LAB}$), selectivity and yield to 2-phenyldodecane ($\sigma_{2\phi}$, $\eta_{2\phi}$) and initial intrinsic activity of the samples ($TOF_0$)

| Sample | $x_{DODEC}$ [%] | $\eta_{LAB}$ [wt.%] | $\sigma_{2\phi}$ [wt.%] | $\eta_{2\phi}$ [wt.%] | $TOF_0$ [$s^{-1}$] |
|---|---|---|---|---|---|
| M0 | 99.0 | 82 | 86 | 70 | 0.019 |
| MH1 | 99.6 | 80 | 87 | 69 | 0.029 |
| MH2 | 98.7 | 81 | 87 | 71 | 0.037 |
| MHF | 99.2 | 83 | 87 | 72 | 0.029 |
| MS6 | 97.9 | 76 | 91 | 69 | 0.085 |

though it has a lower acid sites concentration than the untreated material.

Fig. 5B shows that samples submitted to either steaming (MS) or steaming and mild acid treatment (MS3) feature a very low catalytic activity, while the sample submitted to steaming and strong acid treatment (MS6) shows a dodecene conversion rate of similar magnitude to the one yielded by the parent material. However, when such activity is related to the extremely low acid sites concentration, as measured by pyridine, a substantial increase in the intrinsic activity (TOF) appears, as shown by Table 5. This could be due to the improved accessibility to the acid sites, observed by the increase in the mesoporous surface area shown by the $\alpha_S$-plots of the nitrogen isotherms, as well as by the much lower hydroxylation degree yielded by the steam treatment, which would lead to an improvement in the adsorption rate of the reagents. It can also be seen in Table 5 that MS6 shows a higher selectivity to 2-phenyldodecane than M0, though when this value is combined with its lower yield to linear alkylbenzene, the global yield to 2-phenyldodecane ($\eta_{2\phi}$) remains unchanged.

### 3.1.6. Kinetics

It has been proposed that the kinetics of this reaction follows a first order rate law for dodecene conversion [19]. According to such rate law applied to a batch reactor, it follows that there should be a linear relationship between time and $\ln(1 - x_{DODEC})$, as shown by the equations below:

$$r = -\frac{dC_{DODEC}}{dt} = k \cdot C_{DODEC}$$

$$r = -C^0_{DODEC} \cdot \frac{d(1 - x_{DODEC})}{dt} = k \cdot C^0_{DODEC} \cdot (1 - x_{DODEC})$$

$$-\ln(1 - x_{DODEC}) = k \cdot t$$

However, when such fitting is attempted, though correlations are not bad, deviations are observed for all the samples in the same sense: the low conversion points lie below the fitting straight line, while the high conversion points rise above the fitting line. Accepting the first order law, and being the fitting line slope proportional to the reciprocal of the rate constant ($k^{-1}$), such phenomenon would mean a rate constant lowering throughout the reaction progress, i.e. the deactivation of the catalyst.

Shown in Fig. 6 is the first order fitting for the parent zeolite, compared to the final HCl-dealuminated MHF material (A), and

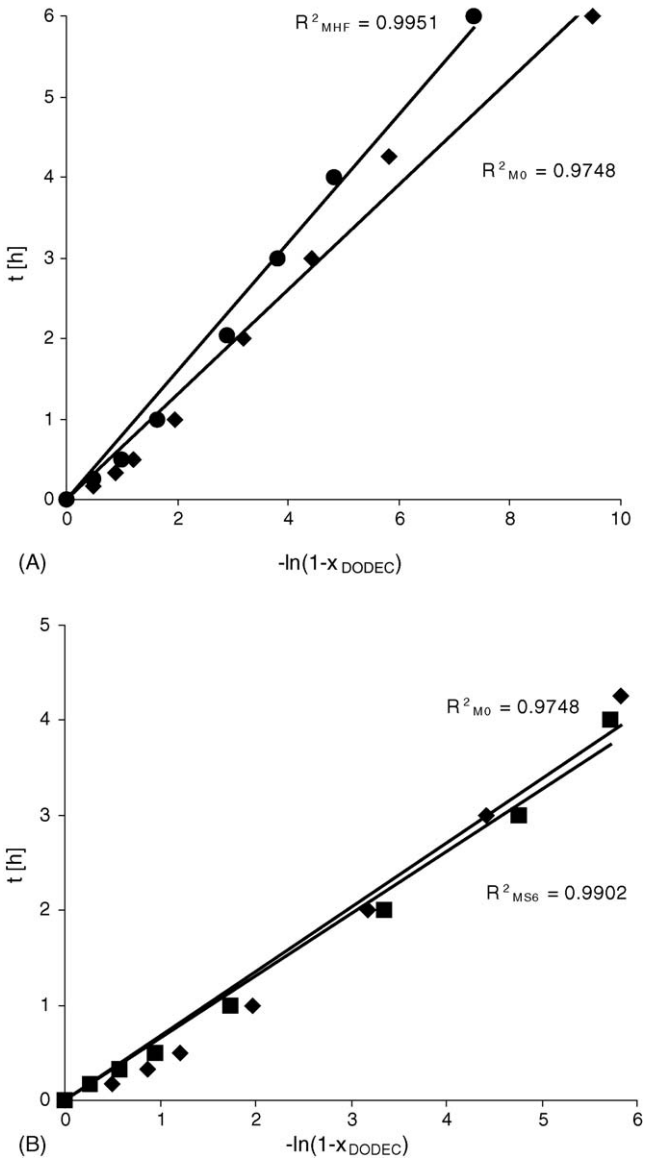


Fig. 6. First order kinetics fitting of final acid-treated (A) and steam-acid treated (B) samples, compared to the parent material: (A) M0, ◆; MHF, ●. (B) M0, ◆; MS6, ■.

to the steam-HCl treated MS6 sample (B). In both cases, it can be seen that a better fitting is achieved with the treated materials. In an attempt to assess the deviation from the first order rate, a non-integer power law fitting was performed, according to the following equations:

$$r = -\frac{dC_{DODEC}}{dt} = k \cdot C^{1+F}_{DODEC}$$

$$r = -C^0_{DODEC} \cdot \frac{d(1 - x_{DODEC})}{dt} = k \cdot (C^0_{DODEC})^{1+F} \cdot (1 - x_{DODEC})^{1+F}$$

$$\frac{1}{(1 - x_{DODEC})^F} - 1 = k \cdot (C^0_{DODEC})^F \cdot F \cdot t$$

This *pseudo* power law kinetics rate expression allows to empirically evaluate the deactivation of the catalyst, as higher values of the $F$ residual term stand for higher relative deactivation rates.

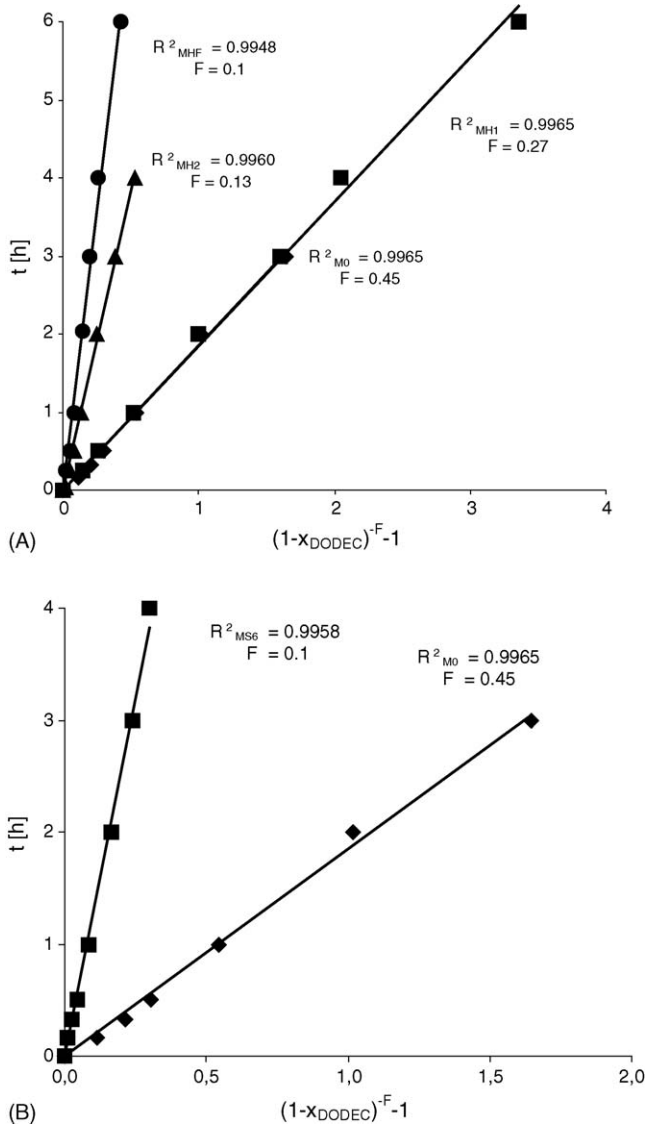


Fig. 7. Optimum *pseudo* order kinetics fittings for acid-treated (A) and steam-acid treated (B) samples, compared to the parent material: (A) M0, ◆; MH1, ■; MH2, ▲; MHF, ●. (B) M0, ◆; MS6, ■.

Fig. 7 presents the optimum fittings for the parent zeolite and the HCl-treated materials MH1, MH2 and MHF (A), as well as the parent zeolite M0 and the steam-acid treated MS6 (B).

It can be seen for the acid-dealuminated materials that the *pseudo* order evolves from 1.4 down to 1.1, i.e. the relative deactivation rate decreases as dealumination increases. It is noticeable that the closest to 1 pseudo order is already achieved with the MH2 sample, whereas further acid dealumination yields no improvement. This result supports the former conclusion that subsequent acid treatment does not modify the catalytic acidity significantly. A similar 1.1 *pseudo* order value is obtained with the steamed and acid leached material MS6.

Another way to assess the relative deactivation rate is to compare the first order kinetic constant ratio at initial time to the values shown at high dodecene conversions. In Table 6, it can be observed that both samples MHF and MS6 showed a noticeable lower first order rate constant decrease (i.e., a higher $k/k_0$ ratio) throughout the reaction when compared to the parent material. This evaluation also shows that although both MHF and MS6 achieved similar *pseudo* order values, there is a substantial improvement in the constant ratio for the steam-acid treated sample, especially when it is taken into account the magnitude of the increase in the number of turnovers needed with the latter material in order to achieve high conversions of dodecene.

Table 6
First order kinetics rate constant decrease at final conversion for chosen samples

| Sample | TON[a] | $k/k_0$ |
|---|---|---|
| M0 | 78 | 0.435 |
| MHF | 138 | 0.504 |
| MS6 | 440 | 0.634 |

[a] Dodecene molecules converted per acid site at final conversion.

When the relative rates of deactivation are examined for the parent material M0 at different temperatures (Fig. 8; Table 7), it can be seen that at 353 K deactivation commands, leading to a steep first rate constant decrease, with no possible fitting for orders between 1 and 2 and yield to linear phenyldodecanes ($\eta_{LAB}$) remaining extremely low. At 373 K, a fitting to a 1.4 *pseudo* order is achieved, along with a noticeable increase in $\eta_{LAB}$ recorded. When temperature reaches 408 K a first order fitting is obtained, along with a further increase in $\eta_{LAB}$. A subsequent temperature increase to 423 K yields no improvement: the *pseudo* order fits to 1.3 and $\eta_{LAB}$ recedes.

The first order rate approximation is suitable for low concentrations at 373, 408 and 423 K. When an Arrhenius plot is made at those temperatures, the apparent activation energy value yielded is 14 kcal mol$^{-1}$ (Fig. 9). When the plot is performed for the steam-acid treated MS6 sample, a mild reduction in the apparent activation energy value occurs, down to 11 kcal mol$^{-1}$. According to the mechanism for the adsorption of alkenes in zeolites proposed by Yoda et al. [34], such effect suggests a change of the rate limiting step for the complex diffusion phenomenon, which could be related to

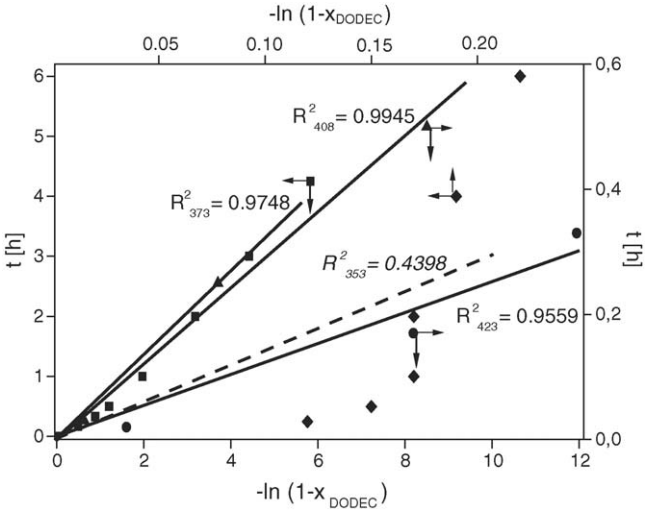


Fig. 8. First order kinetics fitting of the parent material at 353 K (◆), 373 K (■), 408 K (▲) and 423 K (●).

Table 7
Kinetics fitting and yield to linear phenyldodecanes for the parent material (M0) vs. reaction temperature

| $T$ [K] | *Pseudo* order | $\eta_{LAB}$ [wt.%] |
|---|---|---|
| 353[a] | – | 10 |
| 373 | 1.4 | 82 |
| 408 | 1.0 | 85 |
| 423 | 1.3 | 79 |

[a] $x_{DODEC} = 10\%$.

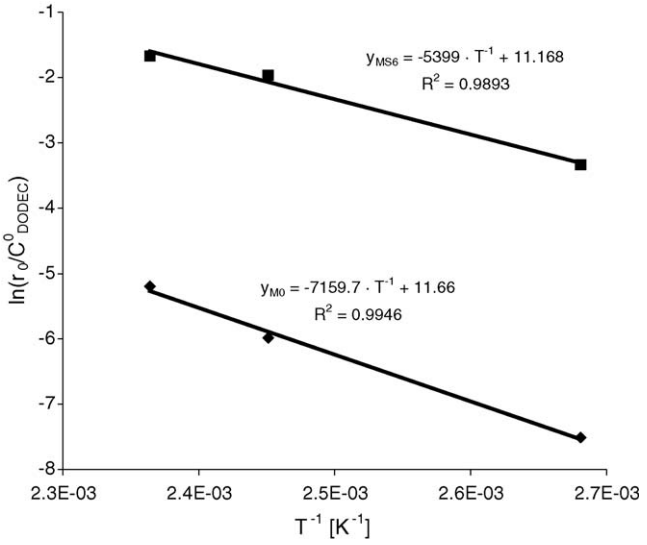


Fig. 9. Arrhenius plots for the parent material (M0, ◆) and the final steam-acid treated sample (MS6, ■).

the change of the hydrophilic properties of the surface yielded by the steam treatment.

## 4. Conclusions

When acid dealumination is carried out in a mordenite, no drastic changes are achieved in terms of either reagents accessibility, as measured by additional porosity generated, or catalytic performance for the alkylation of benzene with 1-dodecene, though acid treated samples show less a tendency to undergo deactivation. When a combined steam-acid treatment is carried out, a noticeable change in the mesoporous area is seen, accompanied by a dramatic increase in the intrinsic activity and a substantial decrease in the deactivation rate of the material, when compared either to the parent material or to the acid-dealuminated samples. This improved behaviour of the steam treated sample is attributed to its lower acid sites concentration and less hydrophilic surface.

## Acknowledgments

The authors would like to thank Dr. M. Faraldos for the priceless help in the $\alpha_S$-plots interpretation and to Prof. J. Pérez-Pariente for his helpful discussions. M.B. thanks Spanish MEC for the FPU grant given. The authors also thank the financial support granted by the Spanish MEC under project MAT2003-07769-C02-02 (Plan Nacional de Investigación Científica, Desarrollo e Innovación Tecnológica).

## References

[1] A.K. Ghosh, J.J. Curthois, J. Chem. Soc., Faraday Trans. 1 (79) (1983) 805.
[2] P. Méariadeau, Y. Ben Taarit, A. Thangaraj, J.L.G. Almeida, C. Naccache, Catal. Today 38 (1997) 243.
[3] J. Scherzer, Catalytic Materials, American Chemical Society, Washington, DC, 1984.
[4] A.W. O'Donovan, C.T. O'Connor, K.R. Koch, Micropor. Mater. 5 (1995) 185.
[5] P.B. Venuto, L. Hamilton, P. Landis, J. Wise, J. Catal. 4 (1966) 81.
[6] Y. Cao, R. Kessas, C. Naccache, Y. Ben Taarit, Appl. Catal. A: Gen. 184 (1999) 231.
[7] J. de Almeida, M. Dufaux, Y. Ben Taarit, C. Naccache, Appl. Catal. A: Gen. 114 (1994) 141.
[8] W. Liang, Z. Yu, Y. Jin, Z. Wang, Y. Wang, M. He, E. Min, J. Chem. Tech. Biotechnol. 62 (1995) 98.
[9] W. Liang, Y. Jin, Z. Yu, Z. Wang, B. Han, M. He, E. Min, Zeolites 17 (1996) 297.
[10] S. Sivasanker, A. Thangaraj, J. Catal. 138 (1992) 386.
[11] R. Ravishankar, T. Sen, V. Ramaswamy, H. Sony, S. Ganapathy, S. Sivasanker, Stud. Surf. Sci. Catal. 84 (1994) 331.
[12] L. Zinner, K. Zinner, M. Ishige, A. Araujo, J. Alloys Compd. 193 (1993) 65.
[13] N. Han, Z. Cui, C. Xu, W. Chen, Y. Jin, Appl. Catal. A: Gen. 238 (2003) 99.
[14] J. Knifton, P.R. Ananteni, P.E. Dai, M. Stockton, Catal. Lett. 75 (2001) 113.
[15] B. Wang, C.W. Lee, T. Cai, S. Park, Bull. Korean Chem. Soc. 22 (2001).
[16] B. Wang, C.W. Lee, T. Cai, S. Park, Catal. Lett. 76 (2001) 99.
[17] A. Nociar, P. Hudec, A. Smiešková, T. Jakubík, Z. Židek, Petroleum Coal 44 (2002) 87.
[18] J. Knifton, P.R. Ananteni, P.E. Dai, M. Stockton, Catal. Today 79–80 (2003) 77.
[19] T. Tsai, I. Wang, S. Li, J. Liu, Green Chem. 5 (2003) 404.
[20] E. Loeffler, U. Lohse, C. Peuker, G. Oehlmann, L.M. Kustov, V.L. Zholobenko, V.B. Kazansky, Zeolites 10 (1990) 266.
[21] B.L. Su, D. Barthomeuf, Zeolites 13 (1993) 626.
[22] I. Kiricsi, C. Flego, G. Panzuconi, W.O. Parker, R. Millini, C. Perego, G. Bellussi, J. Phys. Chem. 98 (1994) 4627.
[23] B.L. Su, V. Norberg, Zeolites 19 (1997) 65.
[24] M. Jiang, H.G. Karge, J. Chem. Soc., Faraday Trans. 92 (1996) 2641.
[25] N.Y. Chen, F.A. Smith, Inorg. Chem. 15 (1976) 295.
[26] M.A. Makarova, J. Catal. 172 (1997) 170;
J. Datka, Zeolites 18 (1997) 245.
[27] P. Bodart, J.B. Nagy, G. Debras, Z. Gabelica, P.A. Jacobs, J. Phys. Chem. 90 (1986) 5183.
[28] H.G. Karge, V. Dondur, J. Phys. Chem. 94 (1990) 765.
[29] C.A. Emeis, J. Catal. 141 (1993) 347.
[30] E. Selli, L. Forni, Micropor. Mesopor. Mater. 31 (1999) 129.
[31] F. Rouquerol, J. Rouquerol, K. Sing, Adsorption by Powders and Porous Solids, Academic Press, London, 1999, p. 204.
[32] T. Keii, T. Tagaki, Anal. Chem. 33 (1961) 1965.
[33] M. Jaroniec, M. Kruk, J.P. Olivier, Langmuir 15 (1999) 5410.
[34] E. Yoda, J. Kondo, K. Domen, J. Phys. Chem. B 109 (2005) 1464.